Supplementary Information (SI) for Nanoscale.
This journal is © The Royal Society of Chemistry 2025

Supplementary Information

Efficient near-infrared and visible regime spatial self-phase modulation in transition metal carbonitride Ti_3CN

Jiawei Cao,[a] Xiaodan Xu,[a] Yixuan Huang,[b,c] Tengdong Zhang,[a] Ying Liu,[a] Haotian Yang,[a] Jimin Zhao,*[b,c,d] Jun Li,*[a] and Yanling Wu*[a]

[a]*State Key Laboratory of Metastable Materials Science and Technology & Hebei Key Laboratory of Microstructural Material Physics, School of Science, Yanshan University, Qinhuangdao 066004, China*
[b]*Beijing National Laboratory for Condensed Matter Physics, Institute of Physics, Chinese Academy of Sciences, Beijing 100190, China*
[c]*School of Physical Sciences, University of Chinese Academy of Sciences, Beijing 100049, China*
[d]*Songshan Lake Materials Laboratory, Dongguan, Guangdong 523808, China*
[†]*Electronic supplementary information (ESI) available.*

*Corresponding author, Email: jmzhao@iphy.ac.cn; ljcj007@ysu.edu.cn; ylwu@ysu.edu.cn

S1. Sample preparation of Ti_3CN flake suspension

The few-layer MXene Ti_3CN dispersion we bought is at the concentration of 5 mg/ml (ultrapure water as the solvent). We dilute the pre-prepared Ti_3CN solution to a concentration of 0.05 mg/ml by adding the solvent ultrapure water. Then we execute a sonicating operation for the solution for 30 minutes (at 40 kHz frequency) to obtain the dispersed suspension, which subsequently is transferred into a standard cuvette with a thickness of 10 mm on standby for SSPM measurements. In parallel, we conducted the control SSPM experiments on solvent, where no SSPM effect was observed.

S2. Key parameters of laser beams in SSPM experiment

A series of continuous-wave laser beams (405, 473, 532, 671, 721, 914 and 1064 nm) are used to investigate SSPM effect. For Gaussian beams, we define the radius of beam waist of the laser incident beam ω_0 is approximately equal to the the $1/e^2$ intensity radius of laser beams. When the beam passes through a lens with a focal length of f = 200 mm, the radius of the beam waist at the focal point is defined as ω_0', where

$\omega_0' \approx \frac{\lambda}{\pi\omega_0} f$. In this work, the distance between the focusing lens and the center of cuvette (l) is fixed at 160 mm. Therefore, the $1/e^2$ intensity radius at the center of cuvette can be calculated by the equation $\omega(z) = \omega_0' \sqrt{1 + \left(z/z_R\right)^2}$, where $\omega(z)$ is the $1/e^2$ intensity radius of laser beam when the distance between the focal point and the center of cuvette is z (here z = 40 mm), $z_R \approx \frac{\pi\omega_0^2}{\lambda}$, the beam area at the center of cuvette is S = $\pi(\omega(z))^2$.

Table S1. Detailed key parameters of laser beams in SSPM experiment.

λ (nm)	ω_0 (mm)	z (mm)	ω_0' (mm)	$\omega(z)$ (mm)	S (mm^2)
405	0.80	40	0.032	0.163	0.0835
473	0.71	40	0.042	0.148	0.0690
532	0.77	40	0.044	0.160	0.0804
671	0.86	40	0.050	0.179	0.1000
721	0.64	40	0.072	0.147	0.0679
914	0.89	40	0.065	0.190	0.1134
1064	0.72	40	0.094	0.172	0.0929

S3. Process of SSPM diffraction rings formation and deformation

For suspension sample, the stable SSPM rings formation includes two processes: one is the process varying from the ring generation until to its maximum in its ring number and diameter, another is the process varying from the maximum rings to the stable deformation rings. Since the second process originate from the thermal-convection-induced ring deformation, we only focus on the first process related to the electron coherence.[1,2] In Fig. S1, as a typical example, we show the evolution process of SSPM diffraction rings of Ti_3CN suspension over the time at 532 nm with the incident intensity of 260.0 W/cm^2. There are two clear processes: One is that the number of rings increases from zero to a maximum taking 0.33 s, which is a nonlinear process of laser-induced electron/hole coherence establishment.[1] Another one is that

the upper half portion of ring patterns begins to collapse from the maximum until stable taking 1.84 s, which is the process of thermal convection-induced ring deformation (thermal effect).[2]

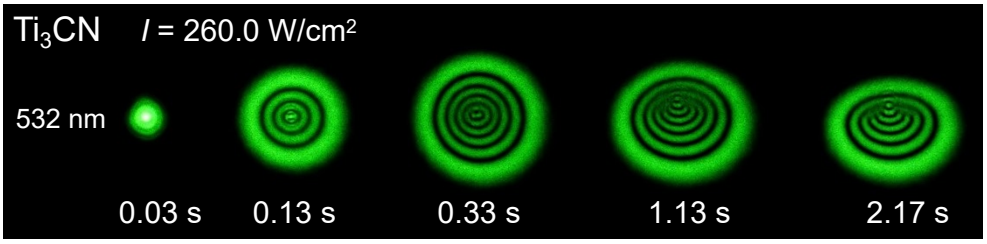

Fig. S1. Process of SSPM diffraction rings evolution over the time for the Ti_3CN flake suspension at 532 nm excitation.

S4. Typical SSPM ring patterns with maximum diameters

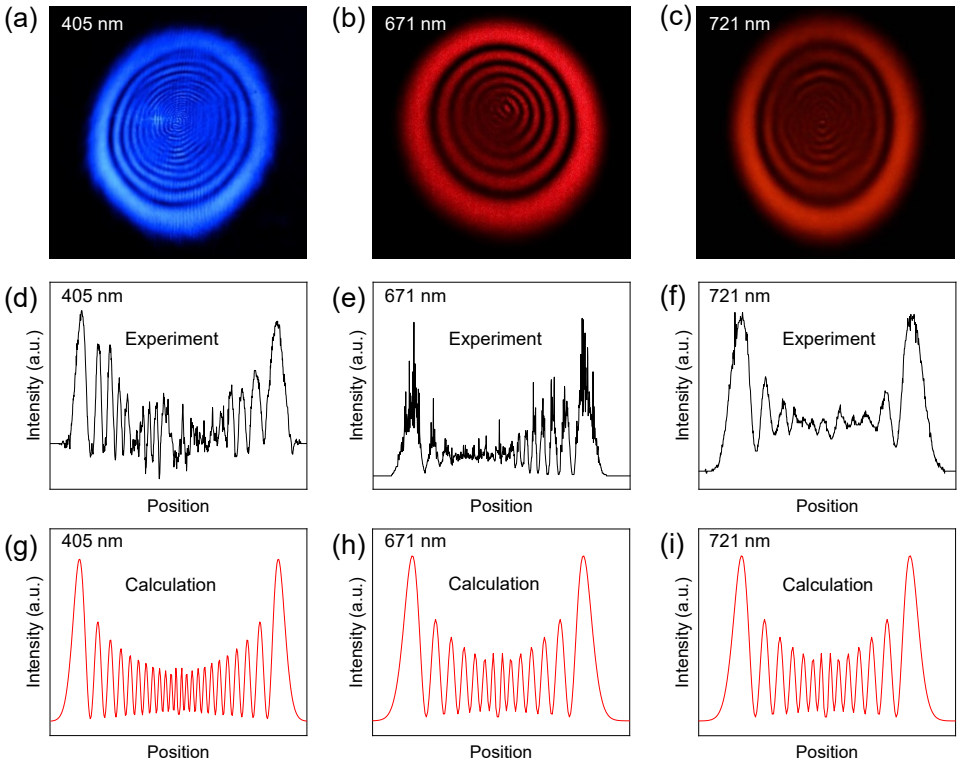

Fig. S2. Typical SSPM ring patterns with maximum diameters under 405 nm, 671 nm and 721 nm laser beam excitation.

S5. Estimation of the effective layer number for Ti_3CN and Ti_3AlCN suspensions

The number of effective layers of the laser beam passing through the Ti_3CN suspension is estimated by the concentration estimation method.[1] The Ti_3CN flakes are

uniformly dispersed in solvent and there is no sediment at the bottom of cuvette. The concentration of the Ti_3CN suspension was ρ = 0.05 g/L (2.948 × 10^{-4} mol/L). The volume of solution contained in the cuvette is $V = 4 \times 10^{-3}$ L. Thus, the total number of molecules in the suspensions is $M = \rho \times V \times N_A = 3.549 \times 10^{17}$ for Ti_3CN. Ti_3CN possesses a crystal structure with the $P6_3/mmc$ space group, where the lattice constants of Ti_3CN are a = 3.02 Å and b = 3.02 Å. Hence, a single effective layer contains $m = S/S_{ab} = S/(\sin 60°)\cdot(a\cdot b) = 5.064\times10^{15}$ molecules for Ti_3CN. The layer number is given by $N_{eff} = M/m$. We estimate the effective layer number to be 70 for Ti_3CN.

S6. Comparison of $\chi^{(3)}_{monolayer}$ values among various 2D materials.

Table S2. Comparison of $\chi^{(3)}_{monolayer}$ among various 2D materials.

Materials	λ [nm]	$\chi^{(3)}_{monolayer}$ [e.s.u.]	References
Ti_3CN	532	5.35×10^{-9}	this work
Ti_3CN	914	5.41×10^{-9}	
Ti_3CN	1064	5.19×10^{-9}	
BP	914	7.28×10^{-9}	3
BP	1064	6.08×10^{-9}	
VP	914	2.11×10^{-9}	
VP	1064	1.81×10^{-9}	
$Ti_3C_2T_x$	532	10^{-7}	4
$Ti_3C_2T_x$	671	10^{-8}	4
$Ti_3C_2T_x$	800	10^{-8}	5
$Ti_3C_2T_x$	1064	10^{-7}	5
Ti_2CT_x	1064	1.14×10^{-10}	6
Nb_2C	400	2.43×10^{-9}	7
Nb_2C	800	6.07×10^{-9}	7
Graphene	532	10^{-7}	2
MoS_2	532	1.60×10^{-9}	1

$MoSe_2$	532	1.10×10^{-9}	8
SnS	532/633	10^{-10}	9
Bi_2Te_3	400/800/1070	10^{-7}	10
$NiPS_3$	532	2.64×10^{-9}	11

S7. Process of SSPM diffraction rings formation

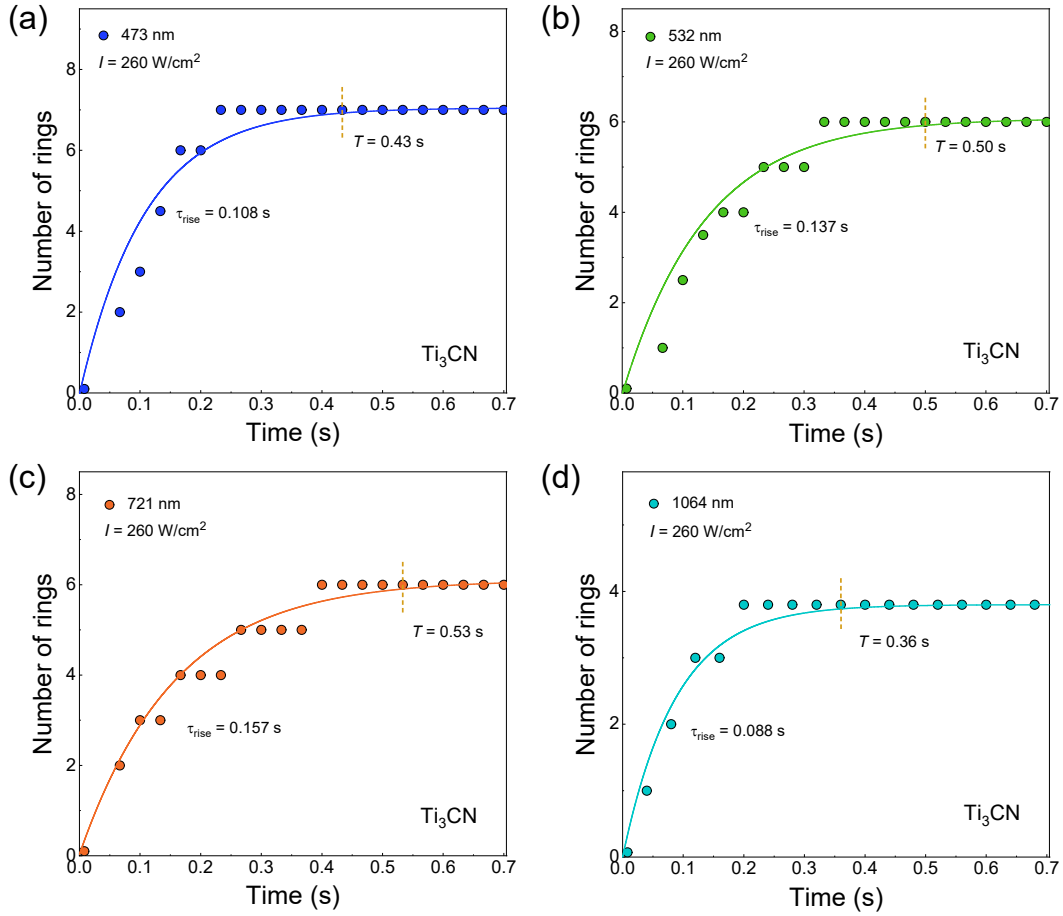

Fig. S3. (a)-(d) Evolution of the ring number over time at 473 nm,532 nm, 721 nm and 1064 nm. Solid lines: fitting curves with one-exponential function. The dashed orange lines denote the formation time.

S8. Calculation Method of Dielectric Constant for Ti_3CN

According to the first principles calculation based on DFT, we obtained the optical properties of Ti_3CN through the Vienna Ab-initio Simulation Package (VASP) program.[12] The exchange and correlation potentials were Perdew-Burke-Ernzerhof

method based on generalized gradient approximation (GGA). The plane wave cut-off energy in the wave vector K space was set to be 700 eV, a Monkhorst-Pack k lattice with a spacing of $2\pi\times0.03$Å^{-1} was employed. When the total energy was stabilized within 1×10^{-8} eV, the force on each atom of the cell after optimization was less than 0.015 eV/Å. Hence, the real part of dielectric function ε as a function of photon energy is shown in Fig. S4.

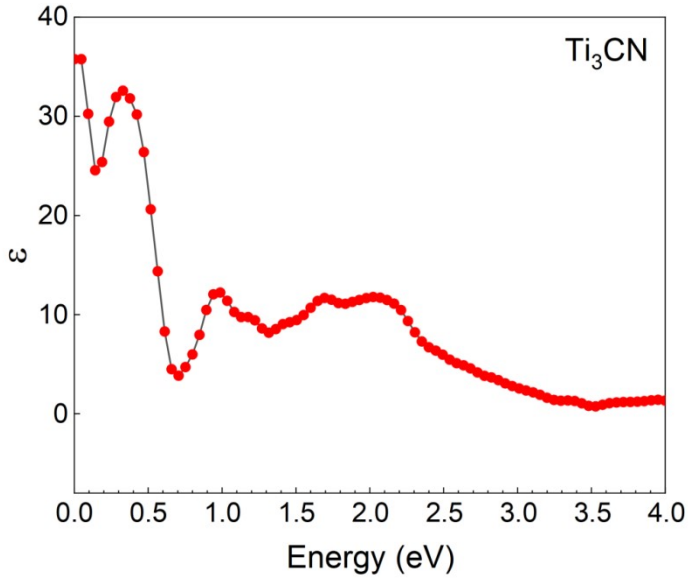

Fig. S4. Real (ε) part of dielectric function obtained through calculation as a function of photon energy for Ti_3CN.

References

1. Y. L. Wu, Q. Wu, F. Sun, C. Cheng, S. Meng, and J. M. Zhao, Proc. Natl. Acad. Sci. U. S. A., 2015, **112**, 11800-11805.
2. R. Wu, Y. L. Zhang, S. C. Yan, F. Bian, W. L. Wang, X. D. Bai, X. H. Lu, J. M. Zhao, and E. G. Wang, Nano Lett., 2011, **11**, 5159-5164.
3. X. D. Xu, M. Wang, Y. Q. Zhang, Q. F. Li, W. S. Niu, Y. F. Yang, J. M. Zhao, and Y. L. Wu, Laser Photon. Rev., 2024, **18**, 2300930.
4. L. M. Wu, X. T. Jiang, J. L. Zhao, W. Y. Liang, Z. J. Li, W. C. Huang, Z. T. Lin, Y. Z. Wang, F. Zhang, S. B. Lu, Y. J. Xiang, S. X. Xu, J. Q. Li, and H. Zhang, Laser Photon. Rev., 2018, 12, 1800215.

5. J. Li, Z. L. Zhang, J. Yi, L. L. Miao, J. Huang, J. R. Zhang, Y. He, B. Huang, C. J. Zhao, Y. H. Zou, and S. C. Wen, Nanophotonics, 2020, **9**, 2415-2424.
6. J. Yi, J. Li, S. H. Huang, L. Y. Hu, L. L. Miao, C. J. Zhao, S. C. Wen, V. N. Mochalin, and A. M. Rao, InfoMat, 2020, **2**, 601-609.
7. S. Xiao, Y. L. He, Y. L. Dong, Y. D. Wang, L. Zhou, X. J. Zhang, Y. W. Wang, and J. He, Front. Physics, 2021, **9**, 674820.
8. W. H. Wang, Y. L. Wu, Q. Wu, J. J. Hua, and J. M. Zhao, Sci Rep, 2016, **6**, 19637.
9. L. M. Wu, Z. J. Xie, L. Lu, J. L. Zhao, Y. Z. Wang, X. T. Jiang, Y. Q. Ge, F. Zhang, S. B. Lu, Z. N. Guo, J. Liu, Y. J. Xiang, S. X. Xu, J. Q. Li, D. Y. Fan, and H. Zhang, Adv. Opt. Mater., 2018, **6**, 1700985.
10. B. X. Shi, L. L. Miao, Q. K. Wang, J. Du, P. H. Tang, J. Liu, C. J. Zhao, and S. C. Wen, Appl. Phys. Lett., 2015, **107**, 151101.
11. J. Li, W. S. Niu, X. D. Xu, M. Wang, Z. W. Xu, J. W. Cao, Y. Liu, J. M. Li, J. M. Zhao, and Y. L. Wu, Opt. Express, 2025, **33,** 1044-1057.
12. P. E. Blochl, Phys. Rev. B., 1994, **50**, 17953-17979.